RSC Advances

This is an *Accepted Manuscript*, which has been through the Royal Society of Chemistry peer review process and has been accepted for publication.

Accepted Manuscripts are published online shortly after acceptance, before technical editing, formatting and proof reading. Using this free service, authors can make their results available to the community, in citable form, before we publish the edited article. This *Accepted Manuscript* will be replaced by the edited, formatted and paginated article as soon as this is available.

You can find more information about *Accepted Manuscripts* in the Information for Authors.

Please note that technical editing may introduce minor changes to the text and/or graphics, which may alter content. The journal's standard Terms & Conditions and the Ethical guidelines still apply. In no event shall the Royal Society of Chemistry be held responsible for any errors or omissions in this *Accepted Manuscript* or any consequences arising from the use of any information it contains.

ROYAL SOCIETY OF CHEMISTRY

www.rsc.org/advances

CREATED USING THE RSC ARTICLE TEMPLATE (VER. 3.1) - SEE WWW.RSC.ORG/ELECTRONICFILES FOR DETAILS

ARTICLE TYPE www.rsc.org/xxxxxx | XXXXXXXX

Preparation and characterization of TiO_2-graphene@Fe_3O_4 magnetic composite and its application on the removal of trace microcystin-LR

Yulu Liang[a,b], Xiwen He[a,b], Langxing Chen *[a,b] and Yukui Zhang[a,b,c]

Received (in XXX, XXX) Xth XXXXXXXXX 200X, Accepted Xth XXXXXXXXX 200X
First published on the web Xth XXXXXXXXX 200X
DOI: 10.1039/b000000x

Microcystins(MCs), a family of potently cyclic heptapeptides, are produced by cyanobacteria blooms in eutrophic water and can cause acute and chronic toxicity even mortality to animal and humans. There existed some strategies for removal of MCs, which only concerned about the highly contaminated water whose concentration of the pollutant was considerably larger than that in nature world. Herein, we developed a ternary composite of TiO_2-coated magnetic graphene and used it as adsorbent and photocatalyst to remove microcystin-LR (MC-LR) from water efficiently. The two-dimensional sheets of graphene were decorated by a large quantity of spherical Fe_3O_4 nanoparticles (10-20 nm) and then coated by crystallized TiO_2. These TiO_2-graphene@Fe_3O_4 composites exhibited a high magnetic response to external magnetic field. And the huge surface of graphene dramatically boost the adsorbability and the charge mobility which lowers the recombination rate of electron–hole pairs and hence systematically enhances the photocatalytic activity. The combination of adsorption and photodegradation provide the composite better performance on the removal of trace amout of MC-LR than commercial photocatalyst Degussa P25. The concentration of MC-LR can be lowered to less than 1μg L^{-1} (a provisional safety guideline by WHO) from 500μg L^{-1} under UV light in 30 min. The loading of TiO_2-graphene@Fe_3O_4, pH and UV energy were also optimized. Moreover, the stable removal capability of TiO_2-graphene@Fe_3O_4 were comfirmed over multiple recycling. Finally the removing performance was also evaluated under solar light illumination in real surface water samples. This work would pave the way for the development of more efficient and easily separable purifier to remove pollutants and toxins in contaminated water.

1. Introduction

With the intensification of anthropogenic activities, especially the untreated industrial sewage and agricultural runoff, eutrophication becomes a growing threat to global aquatic ecosystems[1]. One of the numerous negative consequences is a rapid increase in the frequency of occurrence of cyanobacteria blooms which can potentially produce harmful substances such as cyanotoxins with adverse health effects on living biota[2,3]. Microcystins(MCs), a family of potently cyclic heptapeptides, are the most common cyanotoxins widespread in eutrophic water, particularly their derivative known as microcystin-LR(MC-LR)[4]. These toxins can damage the nervous system or liver and thus cause acute and chronic toxicity or even mortality to humans and animals who come into contact with MCs-contaminated water[5]. Because of the potential toxicity of MC-LR, the World Health Organization(WHO) has proposed a provisional safety guideline of 1 μg L^{-1} in drinking water[6]. Various methods have been used to deal with the MCs removal, but conventional water treatment processes (e.g. coagulation, flocculation and filtration) have been proven to be unreliable or less effective for the elimination of these toxins due to their chemical stability and resistance to a range of pHs[7,8]. Advanced treatment processes such as ultra- and nano-filtration[9] activated carbon absorption[10], pre-ozonation and photo-irradiation Chemical processes that use oxidising agents such as ozone[11], potassium permanganate[12] and chlorine[13] have successfully removed microcystins, but they are either cost-effective or have a risk of side effects [14].

Advanced Oxidation Processes (AOPs) is a reasonable alternative for the removal of many organic contaminants for water and air purification[15], especially the heterogeneous photocatalysis degradation mediated by titanium dioxide (TiO_2)[16-20]. Anatase TiO_2, as the most studied semiconductor photocatalysts, has attracted significant attentions owing to its high efficiency, non-toxicity, low cost, physical and chemistry stability, and environmental ''green'' characteristics [21-24]. Generally speaking, the anatase TiO_2 can generate electron–hole pair when exposed to ultraviolet (UV) irradiation, and then the positive holes and the electrons can react with adsorbed H_2O and O_2 to form hydroxyl radicals(•OH) and superoxide radicals(•O_2) which have highly reactive activities, resulting in the degradation of most organic compounds, including MCs[25,26] (Scheme 1). However, the application of

[a]*State Key Laboratory of Medical Chemical Biology, Research Center for Analytical Science, College of Chemistry, Nankai University, Tianjin 300071, P.R. China. Fax: 86 22 23502458; E-mail: lxchen@nankai.edu.cn*
[b]*Collaborative Innovation Center of Chemical Science and Engineering (Tianjin)*
[c]*Dalian Institute of Chemical Physics, Chinese Academy of Sciences, Dalian 116023, P. R. China. E-mail: ykzhang@dicp.ac.cn*

RSC Advances Accepted Manuscript

pure TiO_2 is limited, owing to its low quantum efficiency[28], poor adsorptive power[29], narrow light absorbance range[30] and difficult separation from water[31].

In the last decade, various strategies have been developed to suppress the recombination of photogenerated electron–hole pairs in TiO_2. In the organic pollutants degradation using TiO_2 as photocatalyst, the substrate could be adsorbed on the inert support for TiO_2 loading and the photodecomposition rate of TiO_2 was affected by the absorption capability of the support[32]; and some of toxins or dyes were also absorbed rather than decomposed[33-36]. The difference between adsorption sites and photoactive sites on the TiO_2 surface and the importance of surface migration of substrates was illustrated. Graphene, due to its atomic sheet of sp^2-bonded carbon atoms arranged into a honeycomb crystal lattice[37], has several excellent attributes, such as the large theoretical specific surface area[38],the high transparency[39], the unique electrical conductivity, high mechanical flexibility, and especially its adsorption activity[40,41]. In particular, graphene oxide (GO), as a novel cousin of graphene, has oxygen-containing groups which enable GO to exhibit excellent hydrophilic properties and rich intercalation chemistry[42,43], making it a highly functional substrate with abundant anchoring sites for efficiently binding with TiO_2 photosensitizers[44]. The graphene−based TiO_2 photocatalysts exhibit systematically enhanced photocatalytic activity: photogenerated electrons are scavenged and subsequently transported by GO after excitation in the conduction band of TiO_2 by UV illumination[45], generating a greater density of electron/hole pairs for high quantum efficiency[46]; Furthermore, the huge surface of graphene dramatically boost the adsorbability and hence systematically enhances the photocatalytic activity[47]. Recent reports indicated that hybridizing TiO_2 nanoparticles with graphene had showed a higher photocatalytic activity than Degussa P25 or pure TiO_2[5,46-53].

Magnetic graphene, the graphene decorated with magnetic iron oxide nanoparticles (NPs), has desirable rapid magnetic response[54] and has been widely applied in the biomedical field, including uses in bioseparation, medical diagnosis, and magnetically targeted drug delivery, as well as in magnetic energy storage, magnetic, fluids, catalysis[55]. However up to now, no report has concentrated on its application in photocatalysis field, though it will potentially improve the separation, recovery and reuse of the photocatalyst and optimize the photodegration[56-59].

Herein, we developed a ternary composite of TiO_2-coated magnetic graphene (TiO_2-graphene@Fe_3O_4) and used it as an efficient and recyclable agent to remove the trace amount of hazardous compound microcystin-LR from aqueous solutions. Due to its adsorptive and photocatalytic properties, TiO_2-graphene@Fe_3O_4 was found to have superior removal performance in comparsion with commercial Degussa P25. Moreover, the composite's removal performance was also effective in multiple recycling. It is expected that the proposed magnetic photocatalyst would pave the way for the development of more efficient and easily separable agent to deal with pollutants and toxins in contaminated water.

2. Experimental

2.1 Materials

All reagents were at least of analytical grade and used without further purification. Graphene oxide (GO) was provided by Nanjing XFNANO Materials Tech. Co. Ltd, China. Tetrabutyl titanate (TBOT) was purchased from Heowns Business License Co. Ltd. Iron (III) chloride hexahydrate ($FeCl_3 \cdot 6H_2O$), sodium acetate, ethylene glycol, ethylene diamine, and anhydrous ethanol were all purchased from Tianjin Chemical Reagent Company (Tianjin, China). Degussa P25 (Degussa AG, Germany) was used as standard materials for comparison purposes. Microcystin-LR (≥95% by HPLC) was purchased from Enzo Life Science Co. Ltd and stored at −20℃. Solutions with an initial concentration of 50 μg L^{-1} were prepared in methanol and employed in all experiments. Trifluoroacetic acid (TFA, 99.5+%, HPLC grade) was purchased from Alfa Aesar. HPLC-grade methanol and acetonitrile (JT Baker) were used in the chromatographic analyses. Highly purified water was prepared with a Milli-Q water purification system (Millipore, Milford, MA).

2.2 Preparation of graphene@Fe_3O_4 composite by solvothermal reaction

The magnetic graphene was prepared according to a modified solvothermal reaction[55]. In a typical procedure, graphene oxide (50mg) was dissolved into ethylene glycol (25mL), followed by addition of $FeCl_3 \cdot 6H_2O$ (0.5g), NaAc (1.5g, as a protective agent) and ethylene diamine (5mL) to form a homogeneous solution under ultrasonic dispersion. The mixture was transferred into a Teflon-lined stainless steel autoclave for solvothermal reaction at 200°C for 16h. After cooled down to room temperature, the black product was collected by a magnet and washed with highly purified water, ethanol for several times, and dried at 50°C in oven for further use.

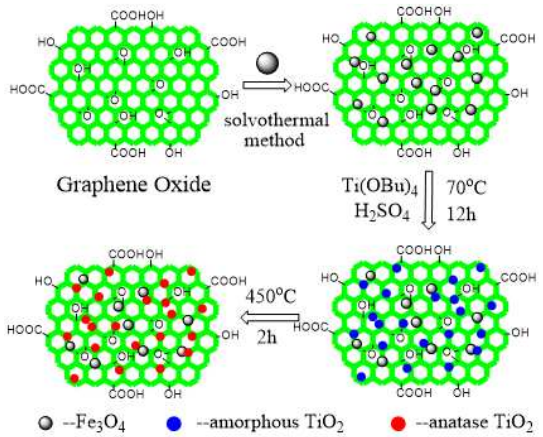

Scheme 1. The synthesis route of TiO_2-graphene@Fe_3O_4 composite.

2.3 Preparation of functionalized TiO_2-graphene@Fe_3O_4 composite

The TiO_2-graphene@Fe_3O_4 composite was synthesized by directly coating TiO_2 layer on the surface of

RSC Advances Accepted Manuscript

This journal is © The Royal Society of Chemistry [year]

graphene@Fe_3O_4[60]. Briefly, the as-prepared magnetic graphene (50 mg) was dispersed in alcohol/water (v/v, 140 ml/10 mL) mixture under ultrasonic for 10 min, and heated to 70°C. Then, $Ti(BuO)_4$ (3 mL) and H_2SO_4 (1 mL) were added in and the solution was mechanically stirred for 12 h at the same temperature. The product, amorphous TiO_2-graphene@Fe_3O_4, was washed with ethanol and water for three times and recovered by magnetic separation. Finally, the dried particles were calcined at 450°C for 2h in air atmosphere to improve the crystallinity of TiO_2.

2.4 Removal Experiments of MC-LR

The removal experiments of MC-LR were performed in a glass vessel reactor containing 20.0 mL MC-LR solution with an initial concentration of 500.0 μg L^{-1}. The pH of the solution was adjusted to 6.0 with TFA; a known concentration (0.50 g L^{-1}) of TiO_2-graphene@Fe_3O_4 and commercial Degussa P25 were dispersed under ultrasonication for 1 min, respectively. For comparison, the experiment of the same mixture stirring in the dark was carried out. The photodegradation was induced by a 125 W mercury vapour lamp positioned at 15 cm from the solution (under constant stirring) in a dark box. A series of aqueous solution (0.50 mL) were sampled using a magnet to remove the suspended catalyst particles at given time intervals.

2.5 HPLC Analytical Procedures

The concentration of MC-LR was measured by high-performance liquid chromatography (HPLC). The obtained samples were analyzed on an Agilent Series 1100 system equipped with a photodiode array detector (PDA) set at 238 nm. The HPLC was carried out under reverse phase condition[19,48], and a C_{18} column (4.6 mm×150 mm, 5μm particle size) was utilized. The mobile phase in isocratic method, a mixture of 0.05% (v/v) trifluoroacetic acid (TFA) in acetonitrile solution and 0.05% (v/v) TFA in MilliQ water at 40:60 ratio，was used to analyze with the flow rate of 1 mL min^{-1}. The injection volume was 50 μL and the temperature of the column was set at 40°C. Under these conditions MC-LR eluted at about 6.7 min. The concentration change of MC-LR follows Lambert–Beer's law (Figure S1, see Electronic supplementary information, ESI).

2.6 Characterization

The morphology and structure of the sythesized magnetic composites were evaluated using a Tecnai G2T2 S-TWIN transmission electron microscope (TEM). Samples for TEM were prepared by placing a drop of dilute nanoparticles of solution in the ethanol solvent on a copper grid. The infrared spectra were recorded on a Nicolet AVATAR-360 Fourier transform infrared (FT-IR) spectrometer. After vacuum drying, the samples were thoroughly mixed with KBr (the weight ratio of sample/KBr was 1%) in a mortar, and then the fine powder was pressed into a pellet. Raman spectra were measured by a FT-Raman microspectrometer (BRUKER RFS100/S, Germany) with a 1046 nm laser with the laser power at 40mW. The identification of the crystalline phase was performed on a Rigaku D/max/2500v/pc (Japan) X-ray diffractometer with a Cu Ka source. The 2θ angles probed were from 3° to 80° at a rate of 4°min^{-1}. The magnetic properties were analyzed with a vibrating sample magnetometer (VSM) (LDJ 9600-1, USA). The X-ray photoelectron spectra were obtained on a Shimadzu (Japan) Kratos AXIS Ultra DLD X-ray photoelectron spectrometer (XPS) with Mg Ka anode (15 kV, 400 W) at a takeoff angle of 45°. The source X-rays were not filtered and the instrument was calibrated against the C1s band at 285eV.

3. Result and Discussion

3.1 Preparation and Characterization of TiO_2-graphene@Fe_3O_4 composite

The synthesis route of TiO_2-graphene@Fe_3O_4 composite is illustrated in Scheme 1. Firstly, the graphene@Fe_3O_4 composites were prepared via a one-step hydrothermal method as described above. The TEM image of graphene@Fe_3O_4 (Figure 1a) showed that two-dimensional graphene oxide (GO) sheets were decorated by a large quantity of spherical Fe_3O_4 NPs. The Fe_3O_4 NPs have an average diameter of approximate 10-20 nm and are well distributed on the surface of GO without serious aggregation. The outline of GO and Fe_3O_4 nanoparticles can be clearly observed. Then, the TiO_2 layer was directly coated on the surface of graphene@Fe_3O_4 and the synthesized TiO_2-graphene@Fe_3O_4 were calcined at 450°C for 2h to improve the crystallinity of TiO_2. The TEM image of TiO_2-graphene@Fe_3O_4 composites (Figure 1b) clearly showed TiO_2 crystals were successfully coated on the surface of graphene@Fe_3O_4, and due to the good chemical and physical stability of graphene, the product still maintain a flake-like structure. Futhermore, compared with Figure 1a, Figure 1b showed the graphene became thicker, and the diameter of Fe_3O_4 inserted in the composite increased from 20 nm to 50 nm, indicating that TiO_2 had been coated on the graphene@Fe_3O_4.

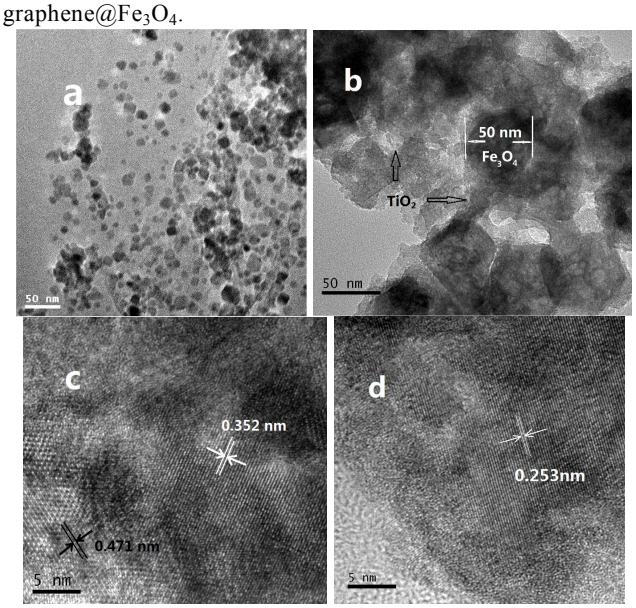

Figure 1 TEM images of the graphene@Fe_3O_4 (a) and the TiO_2-graphene @Fe_3O_4 composite after calcined at 450℃ for 2h (b); HRTEM images of the TiO_2-graphene @Fe_3O_4 (c,d).

RSC Advances Accepted Manuscript

To testify the crystalline phase of TiO_2-graphene@Fe_3O_4, HRTEM micrograph with the lattice fringe information is displayed in Figure 1c and d. Figure 1c showed a well-defined crystallinity of TiO_2 with lattice spacings of 0.352 nm and 0.471 nm, which matched well with the (101) and (001) crystallographic planes of anatase TiO_2. In addition, the crystal lattice fringe with a spacing of 0.253 nm (Figure 1d) can be assigned to the (311) plane of Fe_3O_4. These TEM and HRTEM images were consistent with the XRD results below and offered sufficient evidence proved that Fe_3O_4 and anatase TiO_2 NPs were successfully coated on the GO.

The XRD patterns of the TiO_2-graphene@Fe_3O_4 annealed at 450°C for 2h (c) in an air atmosphere, as well as an unannealed sample (b) and uncoated graphene@Fe_3O_4 (a) are shown in Figure 2. It was observed in each sample that there are six characteristic peaks for Fe_3O_4(2θ=30.2°, 35.5°, 43.1°, 53.5°, 57.1°and 62.7°), and the peak positions at the corresponding 2θ values were indexed as (220), (311), (400), (422), (511), and (440) respectively, which matched well with the database of face centercubic phase of Fe_3O_4 in the JCPDS-International Center for Diffraction Data (JCPDS Card: 19-629) file. The peak intensities of Fe_3O_4 in Figure 2b have partially decreased due to the absorption of X-ray through the TiO_2 shell, indicating amorphous forms of TiO_2. After annealed at 450 ℃, anatase TiO_2 (2θ= 25.3°) is dominant which is the main crystal face (101) of anatase, with other diffraction peaks at 37.8°, 48.1°, 54.7° and 68.8°. These diffraction peaks (marked with symbols "#") are readily indexed to typical anatase TiO_2 crystals (JCPDS No. 21-1272), and the miller indexes of these diffraction peaks are calculated to be (004), (200), (211) and (116), respectively; the other diffraction peaks corresponding to the Fe_3O_4 remained almost the same as those without treatment (Figure 2a). This means that the the graphene@TiO_2 seems to be quite well crystallized, and only TiO_2 in anatase phase is identified, with the interface structure between anatase and magnetite remaining thermodynamically stable.

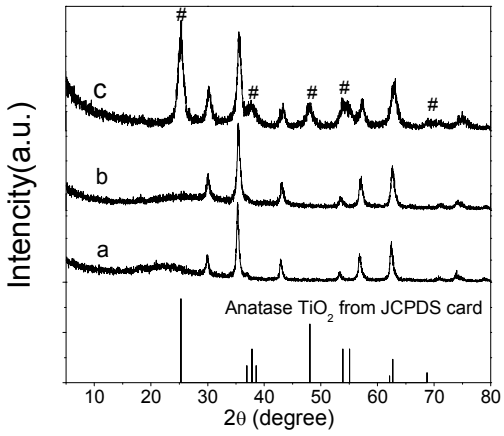

Figure 2 The XRD pattern of uncoated graphene@Fe_3O_4 (a), unannealed TiO_2-graphene@Fe_3O_4 (b), and TiO_2-graphene@Fe_3O_4 annealed at 450°C for 2h in an air atmosphere (c).

Fourier transform infrared (FTIR) spectra of graphene@Fe_3O_4 (a), and TiO_2-graphene@Fe_3O_4 (b) in the range of 4000–450 cm^{-1} were recorded. As exemplified in Figure 3a, the band at 1187.5 cm^{-1}, 1083 cm^{-1} and 877.7 cm^{-1} was due to C−O stretching of the epoxy structures and -COOH in GO, while the bands of 1557.5 cm^{-1} is assigned to C=C stretching vibrations of graphene. The peak at 579.3 cm^{-1} corresponds to the stretching vibration of the Fe–O bond[61] on the graphene@Fe_3O_4. After the introduction of TiO_2 to graphene@Fe_3O_4 (Figure 3b), the intensive peaks at a low frequency (about 572.6 cm^{-1}) were assigned to the combined the effects of Ti-O-C and Ti-O-Ti vibrations, confirming the impregnation of TiO_2 into GO[62], while the peaks at around 2337 cm^{-1} may originate from the dioxide in the air[63]. Compared with Figure 3a, the peaks at 877.7cm^{-1}, 1083.0 cm^{-1} and 1187.5cm^{-1} disappeared, implying that the -COOH and epoxy structures have been replaced by TiO_2. Moreover, the peak at 3422.7 cm^{-1} is ascribed to the O-H stretching frequency from the surface hydroxyl group and the peak at 1629.8 cm^{-1} is attributed to the skeletal vibration of GO sheets, indicative of the structure of GO remained during calcination treatment.

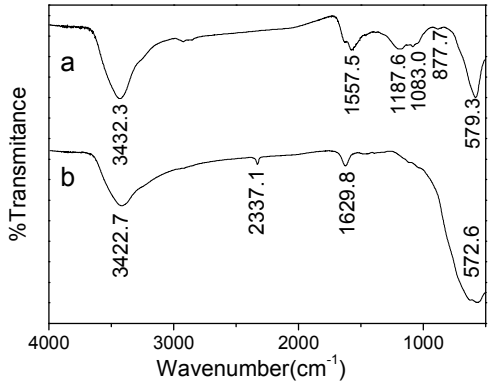

Figure 3 The FTIR spectra of GO@Fe_3O_4 (a) and TiO_2-graphene@Fe_3O_4 (b) composite.

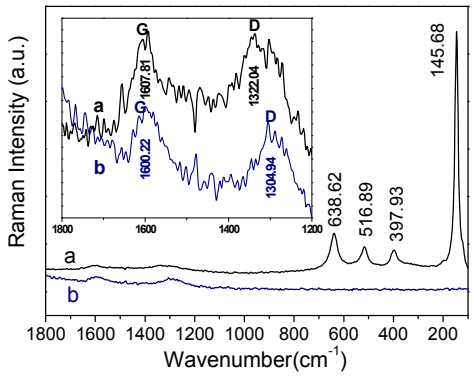

Figure 4 FT-Raman spectra of the TiO_2-graphene@Fe_3O_4 composite (a) and graphene@Fe_3O_4 (b). The inset shows an amplification from 1800 to 1200 cm^{-1}.

The FT-Raman spectra of the Fe_3O_4 NPs, graphene oxide, reduced graphene and graphene@Fe_3O_4 composite were displayed in Figure S2-S3 (see ESI). It can be hardly detected the weak signal of Fe_3O_4, but the variation of location and the

RSC Advances Accepted Manuscript

This journal is © The Royal Society of Chemistry [year]

intensity ratio of D band and G band on the Raman spectra demonstrated the inset of Fe_3O_4 on the surface of graphene. The Raman spectra of the as-prepared TiO_2-graphene@Fe_3O_4 composites was showed in Figure 4. A well resolved TiO_2 Raman peak is clearly seen at about 145.68 cm^{-1}, which is attributed to the main E_g vibration mode of anatase TiO_2, and with other vibration peaks at 397.93 cm^{-1} (B_{1g}), 516.89 cm^{-1} (A_{1g}), and 638.62 cm^{-1} (E_g), it verified the existence of anatase TiO_2 coated on the composite[64]. The result obtained from the Raman spectra was consistent with the XRD results shown in Figure 2b. Additionally, two specific peaks, 1336.84 cm^{-1}(D band) and 1593.40 cm^{-1}(G band), are observed in the spectra (see the inset in Figure 4), which proves the existence of the graphene substrate in both samples. Compared with that of graphene@Fe_3O_4, the marked increase of the D/G intensity ratio for the TiO_2-graphene@Fe_3O_4 composite indicated that a decrease of graphene layers and an increase of more functional groups during the growth of anatase crystallites[65].

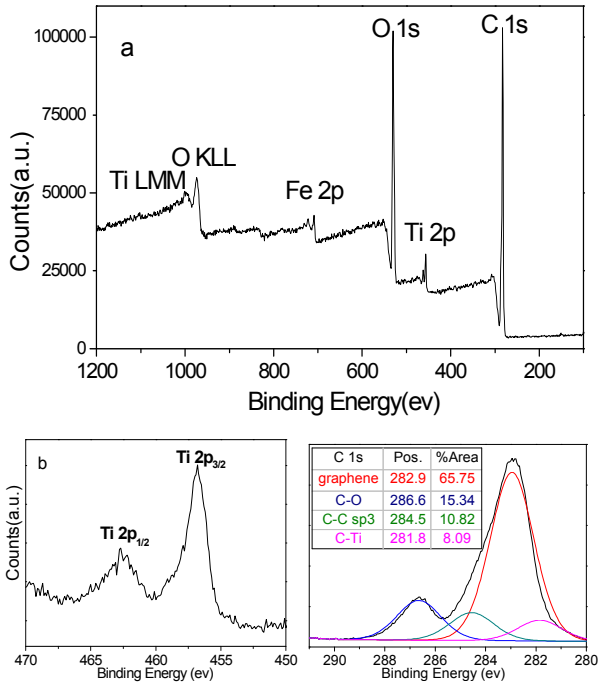

Figure 5 XPS wide-scan spectra(a), high resolution Ti(b) and C1s core-level spectra(c) of the TiO_2-graphene@Fe_3O_4 composites.

XPS was employed to ascertain the composition of the as-prepared TiO_2 immobilized magnetic composites. The wide-scan XPS spectra (Fig. 5a) showed the existence of element C, O and Ti appearing on the surface of TiO_2-graphene@Fe_3O_4 composite. The binding energies of Ti $2p_{3/2}$ and O 1s were 456.8 and 531.7 eV, respectively, which are identical to those for pure TiO_2. The weak intensity of the binding energy at 710.20 eV for Fe 2p further supported that all the Fe_3O_4 nanoparticles in the composite were covered with a shell of titanium oxide. This result was in agreement with above TEM and XRD analysis. The two bands centered at binding energies of 462.7 and 456.8 eV in the composite were attributed to the Ti($2p_{1/2}$) and Ti($2p_{3/2}$) spin–orbital splitting photoelectrons in Ti(Ⅳ), respectively (Figure 5b). However, the energy bonds of the Ti(Ⅳ) were perturbed by the presence of graphene@Fe_3O_4 (shift to low binding energy), which also suggested some substitutions of the Ti-O-Ti by carbon species forming Ti–O–C bonds in the titania lattice[66]. The C1s spectra can be deconvoluted into four individual component peaks, which come from different groups and overlap with each other. The C1s core-level spectrum of TiO_2-graphene@Fe_3O_4 composites was curved into four peak components located at 282.95, 286.65, 284.55, and 281.85eV (Fggure 5c), which are assigned to the C=C in graphene, C-O, sp^3 hybridized C–C[67,68], and C-Ti, respectively. It was noted that the deconvoluted peak at 281.85 eV assigned to the Ti−C bond and the characteristic peak at 286.65 eV attributed to the Ti−O−C bond were consistent with Ti 2p spectra in Figure 5b, indicating the TiO_2 anchored and extended on the surface of graphene sheets[69]. The observation of both crystal lattice and functional groups in the synthesized material further demonstrated the existence of both TiO_2 and magnetic graphene in the composite and intense interactions between the two components.

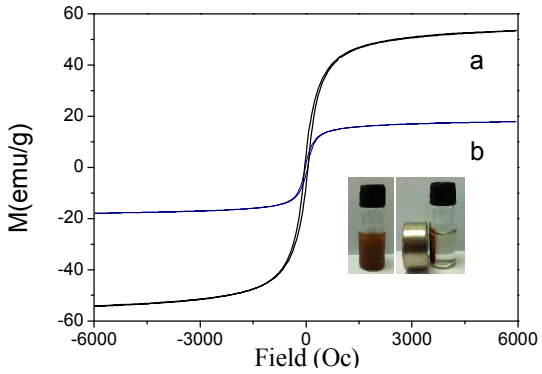

Figure 6 Magnetic hysteresis loops of graphene@Fe_3O_4 (a) and annealed TiO_2-graphene@Fe_3O_4 (b). Magnetic separation-redispersion of TiO_2-graphene@Fe_3O_4 composite is displayed at inset.

The magnetic hysteresis loops of the as-synthesized graphene@Fe_3O_4 and annealed TiO_2-graphene@Fe_3O_4 were displayed in Figure 6. The saturation magnetization (M_s) values of the graphene@Fe_3O_4 and annealed TiO_2-graphene@Fe_3O_4 were 53.7 and 17.9 emu g^{-1} respectively. It was shown that the M_s of the graphene@Fe_3O_4 nanoparticles was significantly higher than that of TiO_2 modified magnetite composite which was attributed to the introduction of the anatase TiO_2 layer which has a very small magnetic susceptibility. However importantly, the remained magnetism of photocatalyst was good enough to easily recover the composites from a suspension by applying an external magnetic field, as shown in Figure 6b. Therefore, it can be almost completely recovered with a minimum loss for many cycles without diminishing both the magnetic property and photoactivity. These properties enabled the material to be highly desirable for the treatment of contaminated waters.

3.2 Removal of MC-LR Compounds by TiO_2-graphene@Fe_3O_4.

RSC Advances Accepted Manuscript

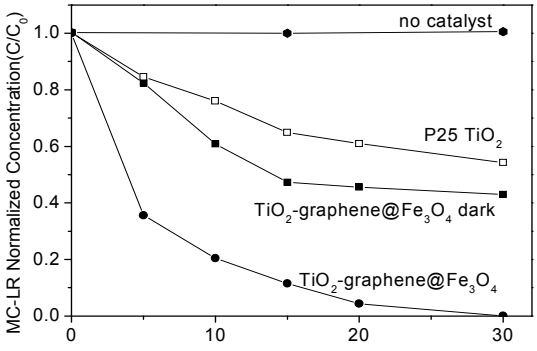

Figure 7 Removal of MC-LR under 125W UV-A (λmax= 365 nm) irradiation in the presence of different nanostructured materials, 0.5 g L^{-1}. Initial MC-LR concentration: 500 μg L^{-1} (pH=6).

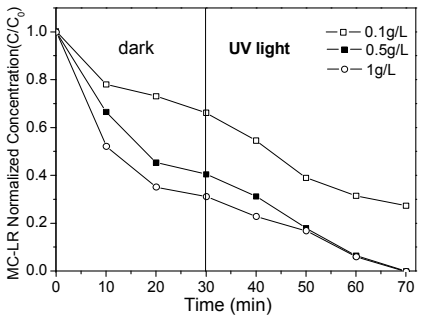

Figure 8 Removal of microcystin-LR with different loadings of TiO_2-graphene@Fe_3O_4 photocatalytic under 125W UV light (λ=365 nm). Initial MC-LR concentration: 500 μg L^{-1} (pH=6).

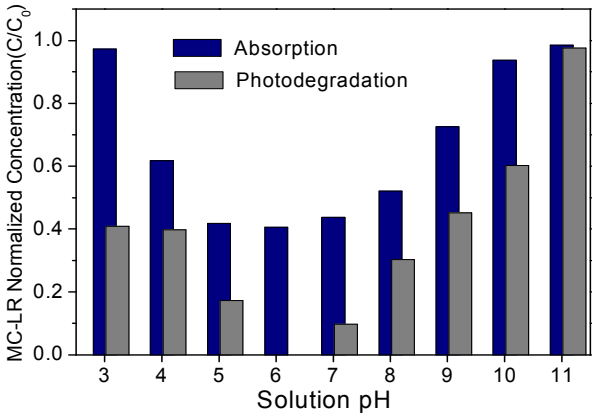

Figure 9 Normalized concentration of MC-LR in solution with 0.5 g L^{-1} photocatalyst after 30 minutes of absorption(blue column) and following 30 minutes of 125W UV irradiation(gray column) with solution pH values ranging from 3 to 11. Initial MC-LR concentration: 500 μg L^{-1}.

The performance of TiO_2-graphene@Fe_3O_4 composites on removing toxins was measured with MC-LR as a model reaction under UV light irradiation, and the results were shown in Figure 7. Control experiment in the absence of catalyst was conducted at weak acidic condition (pH=6) to indicate that the contribution of UV photolysis was negligible since no degradation was observed. It was clear that TiO_2-graphene@Fe_3O_4 under UV (black dots) exhibted more effective performance on removing MC-LR than the commercial Degussa P25 (white square). In all cases, after 30 minutes' UV irradiation, the concentration of MC-LR in the solution with TiO_2-graphene@Fe_3O_4 was reduced to zero (the representative HPLC chromatograms are shown in Figure S4), while 50% MC-LR still remained in the solution with Degussa P25. Experiments performed in the dark (black square) showed that without photodegradation, TiO_2-graphene@Fe_3O_4 adsorbed about 60% toxins and it came to the equilibrium within 30 min. These results indicated that the combination of the adsorption and photodegradation of TiO_2-graphene@Fe_3O_4 is effective to fully remove trace amount of MC-LR.

The absorption and photocatalytic activity of different concentrations of TiO_2-graphene@Fe_3O_4 for the removal of MC-LR from aqueous solutions have been investigated in Figure 8. In the first 30min, we compared the adsorption ability of every sample in the absence of light; and after that, with UV light turned on, a great reduction of MC-LR concentration was observed in next 40 minutes of irradiation time. Expectedly, changing TiO_2-graphene@Fe_3O_4 loading from 0.1 to 0.5 g L^{-1} led to a remarkable increase in both absorption capacity (from 30% to 60%) and the final removal efficiency (from 65% to 100%) of the toxins. A further increase of the loading of ingrdients to 1 g L^{-1} (see white dots) only increased the adsorption loading, but it showed nearly the same efficiency of the MC-LR photocatalytic degradation, thus proving that 0.5 g L^{-1} was the cost-effective concentration of the removal.

As the solution pH has an important effect on the characteristics of the surface electric charges of the catalysts[70], experiments to investigate the absorption and degradation of MC-LR solutions with pH values ranging from 3 to 11 were also carried out. The initial and final pH values were recorded and no change of pH was observed because of the composition change. At first, all the mixtures were incubated in the dark for 30 minutes (to achieve the adsorption equilibrium) to investigate the absorption capacity. From the data of adsorption (blue column) shown in Figure 9, a maximum adsorption was observed at pH 6. When pH of the solution increased or reduced, the absorption capacity of TiO_2-graphene@Fe_3O_4 composite to MC-LR declined. Similar results were observed in previous studies concerning on the absorption of graphene, and the reason may be ascribed to the electrostatic repulsion of the composite and the ionizable groups carried by MC-LR[71]. After 30 minutes' UV irradiation, the MC-LRs in solution of pH 6 was completely removed, while the concentration of MC-LR in other pHs also decreased in varying degrees(see gray column in Figure 9). This results demonstrated that a weak acidic condition (pH=6) was more favorable for the treatment of MC-LR with the TiO_2-graphene@Fe_3O_4 .

RSC Advances Accepted Manuscript

This journal is © The Royal Society of Chemistry [year]

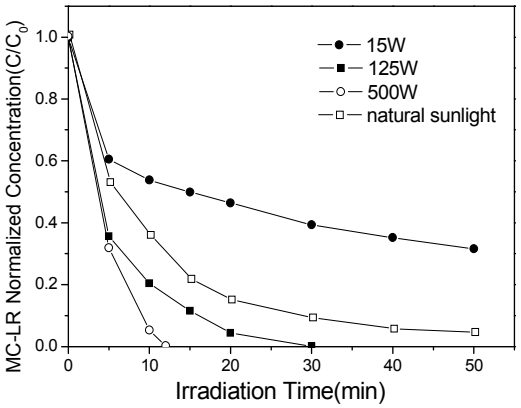

Figure 10 Removal of MC-LR with 0.5 g L^{-1} TiO_2-graphene@Fe_3O_4 photocatalyst under 15W, 125W, 500W UV-light, and natural sunlight. Initial MC-LR concentration: 500 μg L^{-1} (pH=6).

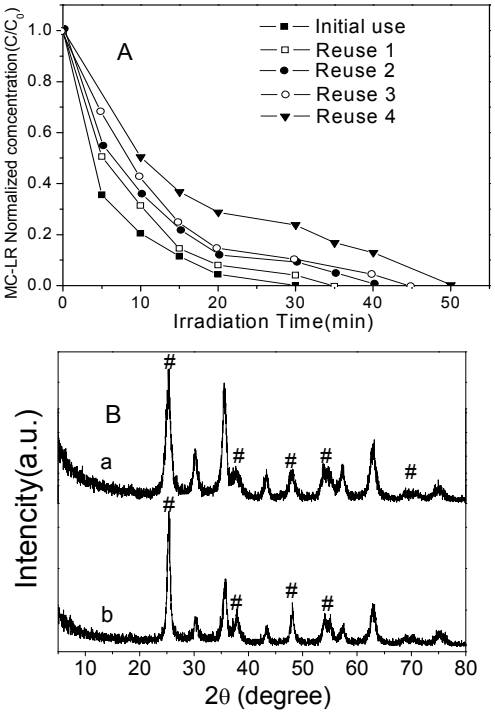

Figure 11 A. Reuse of TiO_2-graphene@Fe_3O_4 for the removal of MC-LR under UV-light. Initial MC-LR concentration: 500 μg L^{-1}; (pH=6). **B.** The XRD pattern of TiO_2-graphene@Fe_3O_4 before(a) and after(b) five cycles of removal reaction of MC-LR.

Three UV sources and natural sunlight have been studied for the MC-LR degradation with TiO_2-graphene@Fe_3O_4 photocatalyst. As shown in the Figure 10, compared with the other two UV sources (15W and 500W), 125W UV light seemed slightly better due to its high efficiency, cost-effective and safety. Besides, sunlight was also a optimum choice to initiate the photodegradation in view of its environmental-friendly property, but it was not quantitative and stable enough to do experimental analysis. Thus, we chosed 125W UV light as light source to deal with our further study, and use sunlight as natural light source treating with the real sample to prove the practical application.

Table 1 Physico-chemical properties of the samples collected from river in Nankai campus.

Physiochemical properties	Sample 1	Sample 2
pH	7.45	7.34
Turbidity(NTU)	1.2	1.1
Dissolved oxygen(%)	123	114
Total Oxygen Carbon(mg L^{-1})	1.8	2.3
Chloride(mg L^{-1})	9.16	9.05
Sulphate(mg L^{-1})	13.5	12.8

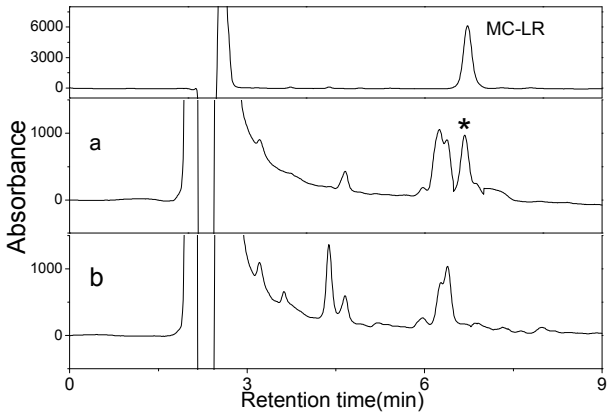

Figure 12 HPLC chromatograms of MC-LR in natural water samples before(a) and after(b) removing reaction of TiO_2-graphene@Fe_3O_4 with natural sunlight.

The reuse of the magnetic composites was subsequently investigated with the optimal loading of TiO_2-graphene@Fe_3O_4 at pH 6. In each cycle, we recycled the composites with an magnet, washed them three times and dried. Prior to every reuse, we weighed the recollected composites to its optimal quantity to make up for the loss of amounts during every sampling and recycle's recovery, so that the result only concerned on the removal performance of the reused magnetic composite. Results summarized in the recycling experiment (Figure 11A) showed the ultimate removal performance has no obvious change in spite that it would take relatively longer time to reduce the concentration to zero. This result, exhibited that the composites could be reused repeatedly and maintain its removal performance over multiple cycles. To further prove the reuse of TiO_2-graphene@Fe_3O_4, the XRD patterns of TiO_2-graphene@Fe_3O_4 before and after five cycles of removal of MC-LR were shown in Figure 11B. The positions of the peaks were identical and only slight decline of peak intensities of anatase TiO_2 were observed, which further demonstrated that the composites possessed reusable and sustainable removal performance during multiple removing processes.

3.3 Practical application

To evaluate the toxins removal performance of the TiO_2-

RSC Advances Accepted Manuscript

graphene@Fe_3O_4 composite in the presence of the natural constituents of water, experiments with surface water were carried out, using natural sunlight irradiation. Surface waters were collected from the river in Nankai campus, and the basic physicochemical parameters of the water were shown in Table 1. In order to simulate an approximate average value of the MC-LR concentration commonly found in water blooms of cyanobacteria, an initial concentration of 50 μg L^{-1} was used as spiked concentration of MC-LR. Irradiation of samples was carried out with sunlight for one hour and TiO_2-graphene@Fe_3O_4 (10 mg L^{-1}) was used as the purifier. The HPLC chromatograms of MC-LR before and after removal reaction are shown in Figure 12, and the complete removing revealed that TiO_2-graphene@Fe_3O_4 had effective removal performance to MC-LR even in natural waters which contain natural organic matters and other constituents.

4. Conclutions

In summary, we developed a ternary recyclable TiO_2-coated magnetic graphene composite and used it as a combination of adsorbent and photocatalyst to remove trace Microcystin-LR toxins. This two-dimensional sheets were decorated by a large quantity of spherical Fe_3O_4 NPs (average 10-20nm and well distributed) and as well coated by crystallized TiO_2. The new composite exhibited a high magnetic response to external magnetic field, high adsorption capbility and excellent photocatalytic activity. Due to the combination of adsorption and photodegradation， 0.5 g L^{-1} of TiO_2-graphene@Fe_3O_4, composite has a better performance on removing trace MC-LR than Degussa P25 at pH 6 under UV irradiation. The concentration of MC-LR could be reduced to 1μg L^{-1} from original 500μg mL^{-1} within 30 minutes. Moreover, the magnetically separable TiO_2-graphene@Fe_3O_4 exhibited a remarkable recycling activity: it can be easily withdrawn from the mixed solution by a small magnet in only 10s, and be separated from solution in subsequent runs with slight loss. The reused composite also maintained its final removal performance over several cycles. Futhermore, real samples test clearly indicated that TiO_2-graphene@Fe_3O_4 was very efficient and effective to remove trace MC-LR even in the real aquatic systems, and under natural sunlight. All the work shows that it the newly sythesized TiO_2-graphene@Fe_3O_4 has a great promising future for practical applications in the environmental protection issues.

Acknowledgements

The authors are grateful to the National Basic Research Program of China (No. 2012CB910601), the National Natural Science Foundation of China (No. 21275080, 21475067), Research Fund for the Doctoral Program of Higher Education of China (No. 20120031110007).

References

1 M.A. Shannon, P.W. Bohn, M. Elimelech, J.G. Georgiadis, B.J. Marinas, and A.M. Mayes, *Nature*, 2008, **452**, 301-310.
2 W.W. Carmichael, *Adv. Bot. Res.*, 1997, **27**, 211-256.
3 J. Pietsch, K. Bornmann, W. Schmidt, *Acta Hydroch. Hydrob.*, 2002, **30**, 7-15.
4 K. Sivonen, *Phycologia*, 1996, **35**, 12.
5 T. Fotiou, T.M. Triantis, T. Kaloudis, L.M. Pastrana-Martínez, V. Likodimos, P. Falaras, A.M.T. Silva, and A Hiskia , *Ind. Eng. Chem. Res.*, 2013, **52**, 13991−14000
6 WHO. Cyanobacterial toxins: microcystin-LR. Guidelines for Drinking-Water Quality; World Health Organization: Geneva, 1998, 95–110.
7 T.P.J. Kull, P.H. Backlund, K.M. Karlsson, J.A.O. Meriluoto, *Environ. Sci. Technol.*, 2004, **38**, 6025–6031.
8 A.M. Keijola, K. Himberg, A.L. Esala, *Toxic Assess*, 1988, **3**, 643–656.
9 A.J. Gijsbertsen-Abrahamse, W. Schmidt, S.G.J. Heijman, *J. Membr. Sci.*, 2006, **276**, 252–259.
10 H.L. Chiang, K.H. Lin, S.Y. Chen, C.G. Choa, S.D. Pan, *Dyes Pigments*, 2007, **75**, 52–59.
11 S. Brooke, G. Newcombe, B. Nicholson, G. Klass, *Toxicon*, 2006, **48**, 1054–1059.
12 E. Rodríguez, M.E. Majado, J. Meriluoto, J.L. Acero, *Water Res.*, 2007, **41**, 102–110.
13 E.M. Rodríguez, J.L. Acero, L. Spoof, J. Meriluoto, *Water Res.*, 2008, **42**, 1744–1752.
14 L.C.V. Jacobs, P. Peralta-Zamora, F.R. Campos, R. Pontarolo, *Chemosphere*, 2013, **90**, 1552–1557.
15 V. K. Sharma, T. M. Triantis, M. G. Antoniou, X. He, M. Pelaez, C. Han, W. Song, K.E. O'Shea, A.A. Cruz, T. Kaloudis, A. Hiskia, and D.D. Dionysiou, *Sep. Purif. Technol.*, 2012, **91**, 3-17.
16 M.G. Antoniou, J.A. Shoemaker, D.D. Dionysiou, A.A. Cruz, *Toxicon*, 2008, **51**, 1103–1118.
17 H. Choi, E.Stathatos, D.D. Dionysiou, *Desalination*, 2007, **202**, 199–206.
18 W.Y. Dong, Y.J. Sun, Q.W. Ma, L. Zhu, W.M. Hua, X.C. Lu, G.S. Zhuang, S.C. Zhang, Z.G. Guo, D.Y. Zhao, *J. Hazard Mater.*, 2012, **229–230**, 307–320.
19 M.G.Antoniou, J.A. Shoemaker, A.A. Cruz, D.D. Dionysiou, *Environ. Sci. Technol*, 2008, **42**, 8877–8883.
20 X. Chen, S.S. Mao, *Chem. Rev.*, 2007, **107**, 2891–2959.
21 A.L. Linsebigler, G.Q. Lu, J.T.Jr. Yates, *Chem Rev.*, 1995, **95**, 735–758.
22 J.C. Liu, H.G. Bai, Y.J. Wang, Z.Y. Liu, X.W. Zhang, D.D. Sun, *Adv. Funct. Mater.*, 2010, **20**, 4175–4181.
23 K. Fuku, T. Kamegawa, K. Mori and H. Yamashita, *Chem.–Asian J.*, 2012, **7**, 1366-1371.
24 B.S. Huang, M.Y. Wey, *Int. J. Hydrogen Energy*, 2011, **36**, 9479-9486.
25 C.M. Maurino, E. Pelizzetti, *Res. Chem. Intermed.*, 1997, **33**, 319-332.
26 P.C. Ma, W. Jiang, F.H.Wang, F.S. Li, P. Shen, M.D. Chen, Y.J. Wang, J. Liu, P.Y. Li, *J.Alloys Compd*, 2013, **578**, 501–506.
27 I. Liu, L.A. Lawton, P.K.J.Robertson, *Environ. Sci. Technol.*, 2003, **37**, 3214-3219.
28 X.F. Yanf, J.L. Qing, Y. Li, R.X. Zhang, H. Tang, *J. Hazard. Mater.*, 2013, **261**, 342–350.
29 J. Zhao, T. Wu, K. Wu, K. Oikawa, H. Hidaka, N. Serpone, *Environ. Sci. Technol.*, 1998, **32**, 2394–2400.
30 A. Di Paola, E. García-López, G. Marcì, L. Palmisano, *J. Hazard. Mater.*, 2012, **211-212**, 3–29.
31 I. Sopyan, M. Watanabe, S. Murasawa, *J Photochem Photobiol., A*, 1996, **98**, 79–86.
32 N. Takeda, T. Torimoto, S. Sampath, S. Kuwabata, and H. Yoneyama, *J. Phys. Chem.*, 1995, **99**, 9986-9991.
33 K.L. Lv and Y.M. Xu, *J. Phys. Chem. B*, 2006, **110**, 6204-6212.
34 Q. Sun and Y.M. Xu, *J. Phys. Chem. C,* 2009, **113**, 12387–12394.
35 Y.M. Xu, K.L. Lv, Z.G. Xiong, W.H. Leng, W.P. Du, D. Liu, and X.J. Xue, *J. Phys. Chem. C*, 2007, **111**, 19024-19032.
36 Q. Sun, Y.M. Xu, *J. Phys. Chem. C,* 2010, **114**, 18911-18918.
37 M. Ishigami, J.H. Chen, W.G. Cullen, M.S. Fuhrer, E.D. Williams, *Nano Letters, 2007, 7,* 1643.
38 M**.J.** McAllister, J.L. Li, D.H. Adamson, H.C. Schniepp, A.A. Abdala, J. Liu, M. Herre*ra-Alonso, D.*L. Mili**u**s, R. Car, R.K. Prudhomme, I.A. Aksay, *Chem.Mater.*, 2007 , **19**, 4396-4404.
39 R.R. Nair, P. Blake, A.N. Grigorenko, K.S. Novoselov, T.J. Booth, T. Stauber, N.M.R. Peres, A.K. Geim, *Science*, 2008, **320**, 1308-1314.

RSC Advances Accepted Manuscript

This journal is © The Royal Society of Chemistry [year]

40 P.V. Kamat, *J. Phys. Chem. Lett.*, 2011, **2**, 242–251.
41 A.K. Geim, *Science*, 2009, **324**, 1530–1534.
42 Z.H. Liu, Z.M. Wang, X.J. Yang, and K. Ooi, *Langmuir*, 2002, **18**, 4926−4932.
43 J.Y. Xu, Y. Hu, L. Song, Q.G. Wang, W.C. Fan, *Mater Res Bull*, 2001, **36**, 1833−1836.
44 S. Morales-Torres, L.M. Pastrana-Martinez, J.L. Figueiredo, J.L.A.M. Faria, Silva, *Environ. Sci. Pollut. Res. Int.*, 2012, **19**, 3676
45 G. Williams, B. Seger, P.V. Kamat, *ACS Nano*, 2008, **2**, 1487-1491.
46 B.S. Huang, F.Y. Chang, and M.Y. Wey, *J. Mol. Catal. A: Chem.*, 2005, **194**, 235.
47 W. Low, V. Boonamnuayvitaya, *J.Environ.Manage.*, 2013, **127**, 142-149.
48 H. Choi, M.G. Antoniou, M. Pelaez, A.A. de la Cruz, J.A. Shoemaker, D.D. Dionysiou, *Environ. Sci. Technol.*, 2007, **41**, 7530–7535.
49 H. Zhang, X.J. Lv, Y.M. Li, Y. Wang, J. H. Li, *ACS Nano*, 2010, **4**, 380–386
50 K.F. Zhou, Y.H. Zhu, X.L. Yang, X. Jiang, C.Z. Li, *New J. Chem.*, 2011, **35**, 353–359.
51 X.Y. Zhang, H.P. Li, X.L. Cui, Y. Lin, *J.Mater. Chem.*, 2010, **20**, 2801–2806.
52 L.M. Pastrana-Martínez, S. Morales-Torres, V. Likodimos, J. L. Figueiredo, J. L.Faria, P. Falaras, A.M.T. Silva, *Appl. Catal. B,* 2012, **123−124**, 241-256.
53 Y.L. Min, K. Zhang, W. Zhao, F.C. Zheng, Y.C. Chen, Y.G. Zhang, *Chem. Eng. J.*, 2012, **193–194**, 203–210.
54 X. Sun, J.P. He, G.X. Li, J. Tang, T. Wang, Y.X. Guo and H.R. Xue, *J. Mater. Chem. C*, 2013, **1**, 765-777.
55 Y.L. Liang, L.X. Chen, X.W. He, Y.K Zhang, *RSC Adv*., 2014, **4**, 18132–18135.
56 W. Fu, H. Yang, L. Chang, B. Hari, M. Li, G. Zou, *Surf. A: Phys. Eng. Aspects*, 2006, **289**, 47–52.
57 W. Fu, H. Yang, M. Li, L. Chang, Q. Yu, J. Xu, G. Zou, *Mater. Lett.*, 2006, **60**, 2723–2727.
58 S. Shylesh, V. Schünemann, W.R. Thiel, *Angew. Chem. Int. Ed.*, 2010, **49**, 3428–3459.
59 A-H. Lu, E.L. Salabas, F. Schüth, *Angew. Chem. Int. Ed.*, 2007, **46**, 1222–1244.
60 Q.H. Min, X.X. Zhang, H.Y. Zhang, F. Zhou, J.J. Zhu, *Chem. Commun.*, 2011, **47**, 11709–11711.
61 H. Zhou, C. Zhang, X. Wang, H. Li, Z. Du, *Synth. Met.*, 2011, **161**, 2199-2205.
62 Y.Y. Gao, X.P. Pu, D.F. Zhang, G.Q. Ding, X. Shao, M. Jing, *Carbon*, 2012, **50**, 4093–4101.
63 D.W.T. Griffith, N.M. Deutscher, C. Caldow, G. Kettlewell, M. Riggenbach, S. Hammer, *Atmos. Meas. Tech.*, 2012, **5**, 2481-2498.
64 Y.L. Min, K. Zhang, W. Zhao, F.C. Zheng, Y.C. Chen, Y.G. Zhang, *Chem. Eng. J.*, 2012,**193–194**, 203–210
65 F. Tuinstra, J. L. Koenig, *J. Chem. Phys.*, 1970, **53**, 1126–1130.
66 G. Williams, B. Sege, P.V. Kamat, ACS Nano, 2008, **2**, 1487–1491.
67 O. Akhavan, *ACS Nano*, 2010, **4**, 4174−4180.
68 S.W. Liu, C. Liu, W.G.Wang, B. Cheng, J. G. Yu, *Nanoscale*, 2012, **4**, 3193−3200.
69 T. Ohsaka, F. Izumi, Y. Fujiki, *J. Raman. Spectrosc.*, 1978, **7**, 321–324.
70 Y.L. Su, Y.R. Deng, L. Zhao, Y.X. Du, *Chin Sci Bull.*, 2013, **58**, 1156-1161.
71 S. Pavagadhi, A.L.L. Tang, M. Sathishkumar, K.P. Loh, R. Balasubramainian, *Water Res.*, 2013, **47**, 4621-4629

RSC Advances Accepted Manuscript